arXiv:1811.01972v1 [cond-mat.mes-hall] 5 Nov 2018

A microwave-assisted spectroscopy technique for determining charge state in nitrogen-vacancy ensembles in diamond

D. P. L. Aude Craik[1], P. Kehayias[1,2], A. S. Greenspon[3], X. Zhang[3], M. J. Turner[1.4], J. M. Schloss[4,5], E. Bauch[1], C. A. Hart[1], E. L. Hu[3], and R. L. Walsworth[1,2,4]

[1]*Department of Physics, Harvard University, Cambridge, Massachusetts, USA*

[2]*Harvard-Smithsonian Center for Astrophysics, Cambridge, Massachusetts, USA*

[3]*John A Paulson School of Engineering and Applied Sciences, Harvard University, Cambridge, Massachusetts 02138, USA*

[4]*Center for Brain Science, Harvard University, Cambridge, Massachusetts 02138, USA and*

[5]*Department of Physics, Massachusetts Institute of Technology, Cambridge, Massachusetts 02139, USA*

We present a microwave-assisted spectroscopy technique for determining the relative concentrations of nitrogen vacancy (NV) centers in diamond that are negatively-charged (NV^-) and neutrally-charged (NV^0). Our method is based on selectively modulating the NV^- fluorescence with a spin-state-resonant microwave drive to isolate, in-situ, the spectral shape of the NV^- and, subsequently, NV^0 contributions to an NV-ensemble sample's fluorescence. The sample-specific nature of this method accounts for any sample-to-sample variations in the spectral shape of the NV^- and NV^0 fluorescence; and permits the investigation of the effect of material parameters, such as local strain and nitrogen concentration, on the steady-state charge-state distribution in NV ensembles. Our method does not rely on a specific illumination sequence, and can be applied with any illumination conditions of interest, as long as they produce fluorescence contrast between the NV^- spin states. The techniques presented here may be generalized to determine relative concentrations of other solid-state defects whose fluorescence can be selectively modulated by means of a microwave drive.

I. INTRODUCTION

Ensembles of negatively-charged nitrogen vacancy centers (NV^-) in diamond are now a leading modality for magnetic field sensing and imaging with high spatial resolution [1–3]. Importantly for diverse applications, NV-diamond magnetometers can operate at ambient conditions and in direct contact with samples that are incompatible with the pressures or temperatures required in atomic or SQUID magnetometry, such as living organisms [4–7], paleomagnetic rocks [8, 9] and temperature-dependent magnetic spin textures and current distributions [3].

However, the sensitivity of ensemble nitrogen-vacancy (NV) diamond magnetometers, currently at $\sim 1\,\mathrm{pT}/\sqrt{\mathrm{Hz}}$ [7, 10], still lags behind that of other methods, in part due to the presence of neutrally-charged NVs (NV^0) in diamond samples. Unlike the negatively-charged defect, which exhibits a spin-dependent fluorescence intensity that can be used to read out its spin state (Fig. 1(a)) via optically-detected magnetic resonance (ODMR), the neutral defect lacks a demonstrated optical method for spin-state readout and hence cannot be used to optically measure and map magnetic fields. Instead, under illumination with the 532-nm light typically used for ODMR of NV^- ensembles, NV^0 defects produce only a spin-independent fluorescence background, which degrades the readout contrast of the NV^- spin state, reducing magnetic field sensitivity.

Material parameters relating to diamond growth and processing are thought to impact the relative concentrations of NV^0 and NV^- defects in a given sample, but this is, as of yet, poorly understood. Further, there is evidence that NV^0 can recombine with electrons in the lattice to form NV^- and NV^- can ionize to NV^0, with recombination and ionization rates depending both on wavelength and intensity of laser illumination [12–16].

Developing new methods to characterize and tune the steady-state charge state of NV en-

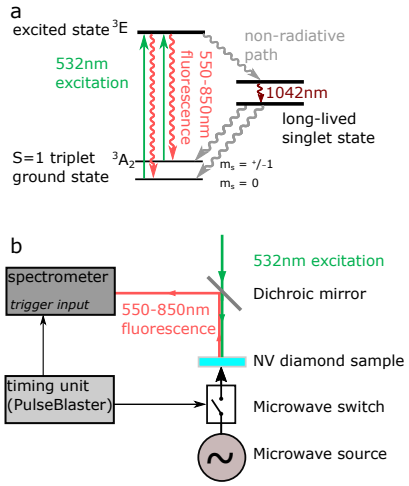


FIG. 1. (a) NV^- energy level structure, which enables optically-detected magnetic resonance (ODMR). Under 532-nm illumination, population in the $m_s = 0$ state cycles in a spin-conserving transition between the ground state and the ^3E excited state, fluorescing brightly when returning to the ground state. In contrast, population in $m_s = \pm 1$ appears dimmer, since it has a $\sim 50\%$ probability of non-radiatively crossing to a metastable singlet state, from whence it decays to the ground state – with slightly higher probability to the $m_s = 0$ spin state – without emitting visible photons [11]. Hence, continuous 532-nm illumination will optically pump population to the $m_s = 0$ state and a microwave drive resonant with the $m_s = 0$ to $m_s = \pm 1$ transition will modulate the fluorescence emitted by NV^- by transferring population between the two spin states. (b) Experimental setup: a confocal microscope is used to illuminate a diffraction-limited spot on an NV diamond sample and to collect its fluorescence, which is directed to a spectrometer by a dichroic mirror. A computer-controlled timing unit (Spincore PulseBlaster card) is used to trigger the acquisition of spectra and to control a microwave switch, which turns on and off a 2.87 GHz microwave drive delivered to the diamond via a small loop antenna. Once triggered, the spectrometer acquires data for an exposure time t_{exp}, typically set between 20 and to 1000 ms, during which time a photoluminescence (PL) spectrum is acquired.

sembles in diamond is therefore crucial. In particular, there is a need for a charge-state-determination method that does not require the application of a specified illumination sequence, but functions instead under any experimental conditions. Such a method can be used to determine what the charge ratio will be when any given experimental protocol of interest is applied.

Further, it has been previously observed that features of the fluorescence spectra of NV^- and NV^0 defects change both as a function of experimental parameters, such as temperature [17] and illumination wavelength [16], and material parameters, such as local strain [18], suggesting that spectra taken from such defects in different samples, or even in different locations in the same sample, may not be comparable. Such variations in spectra are not accounted for in many currently-used methods for charge-state determination, such as taking the ratio of the areas under the NV^0 and NV^- zero-phonon lines (ZPLs) in an NV ensemble photoluminescence (PL) spectrum or using single-NV spectra reported in the literature to fit for the NV^- and NV^0 contributions in another sample's spectrum.

In this paper, we propose a simple method for in-situ determination of steady-state charge-state in an NV ensemble. Our method extracts the NV^- and NV^0 spectra of the ensemble of interest in situ, accounting for any variations due to local environment or experimental conditions. This technique does not rely on a specific illumination sequence and can be applied with any laser excitation that produces a fluorescence contrast between the $m_s = 0$ and $m_s = \pm 1$ spin states of NV^-. It can hence be used to investigate how illumination conditions, material parameters, and other experimental parameters affect charge state in an NV ensemble.

II. METHOD

Our method centers around isolating the NV^- and NV^0 fluorescence contributions to the photoluminescence spectrum emitted by an ensemble of NVs by selectively modulating the

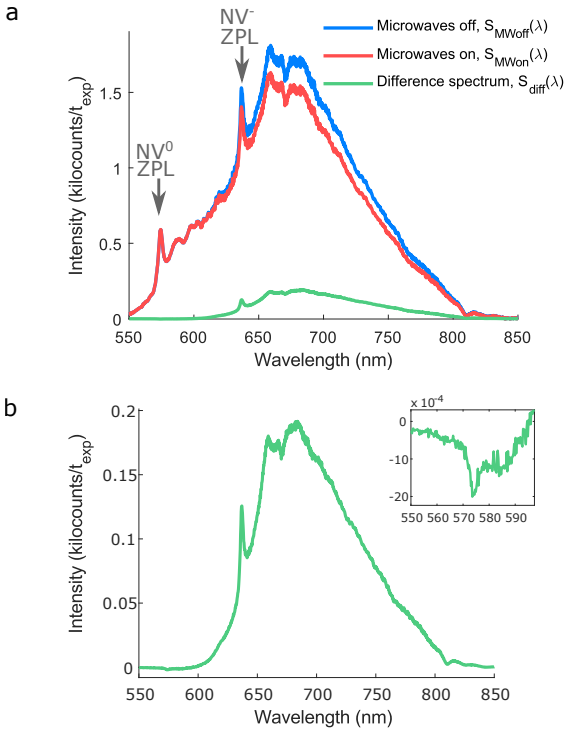


FIG. 2. (a) Measured microwaves-on (red) and microwaves-off (blue) spectra with both the NV^- and NV^0 zero-phonon lines (indicated by grey arrows) visible at 575 nm and 637 nm, respectively. The unscaled difference spectrum (microwaves-off − microwaves-on) is shown in green. (b) Magnified view of the difference spectrum, composed mostly of NV^- fluorescence, except for a small NV^0 contribution due to a spin-dependent ionization effect, which causes a negative NV^0 ZPL signature (magnified in the inset). This spin-dependent ionization effect is corrected for in section II C.

NV^- fluorescence with a microwave drive. We can write the spectrum measured in the absence of a microwave drive, which we will henceforth call the microwaves-off spectrum, $S_{\mathrm{MWoff}}(\lambda)$, in terms of an NV^- and an NV^0 component, as follows:

$$S_{\mathrm{MWoff}}(\lambda) = a_{\mathrm{NV^-}}\hat{S}_{\mathrm{NV^-}}(\lambda) + a_{\mathrm{NV^0}}\hat{S}_{\mathrm{NV^0}}(\lambda) \tag{1}$$

where $\hat{S}_{\mathrm{NV^-}}(\lambda)$ and $\hat{S}_{\mathrm{NV^0}}(\lambda)$ are the pure NV^0 and NV^- spectra, normalized to have unit area (one can think of these as basis spectra) and $a_{\mathrm{NV^-}}, a_{\mathrm{NV^0}}$ are positive constants, representing the area under the NV^- and NV^0 contributions to the total microwaves-off spectrum.

The ratio of NV^- to NV^0 concentration in an NV ensemble, henceforth referred to as the charge-state ratio, R, can be written as:

$$R \equiv \frac{[\mathrm{NV^-}]}{[\mathrm{NV^0}]} = \frac{a_{\mathrm{NV^-}}}{a_{\mathrm{NV^0}}} \cdot \frac{\tau_{\mathrm{NV^0}}}{\tau_{\mathrm{NV^-}}} \tag{2}$$

where $1/\tau_{\mathrm{NV^0}}$, $1/\tau_{\mathrm{NV^-}}$ are the radiative decay rates of NV^0 and NV^- respectively. Our goal is to decompose the total microwaves-off spectrum into its NV^- and NV^0 contributions:

$$\begin{aligned} S_{\mathrm{NV^-}}(\lambda) &= a_{\mathrm{NV^-}}\hat{S}_{\mathrm{NV^-}}(\lambda) \text{ and} \\ S_{\mathrm{NV^0}}(\lambda) &= a_{\mathrm{NV^0}}\hat{S}_{\mathrm{NV^0}}(\lambda) \end{aligned} \tag{3}$$

from which we can determine the ratio of areas, $\frac{a_{\mathrm{NV^-}}}{a_{\mathrm{NV^0}}}$ and find R. This involves three main steps:

1. Isolate the NV^- spectral shape by microwave modulation;

2. Find the correct scale factor by which to multiply the spectral shape of NV^-, to determine the total NV^- contribution to $S_{\mathrm{MWoff}}(\lambda)$;

3. Correct for spin-dependent ionization.

Finding the absolute ratio, R, will also require measuring the radiative lifetimes $\tau_{\mathrm{NV^0}}$ and $\tau_{\mathrm{NV^-}}$ (which can be done using time-correlated photon counting, as previously demonstrated in [19], for example) and calibrating out the effect of any wavelength-dependent losses in the optics setup (using, for instance, a white light source). The subsections which follow describe each of the steps for determining $\frac{a_{\mathrm{NV^-}}}{a_{\mathrm{NV^0}}}$ in detail, and present an example application to photoluminescence data taken at a confocal spot on a bulk NV ensemble in a chemical-vapor-deposition-grown diamond sample (refer to the technical supplement for further technical details).

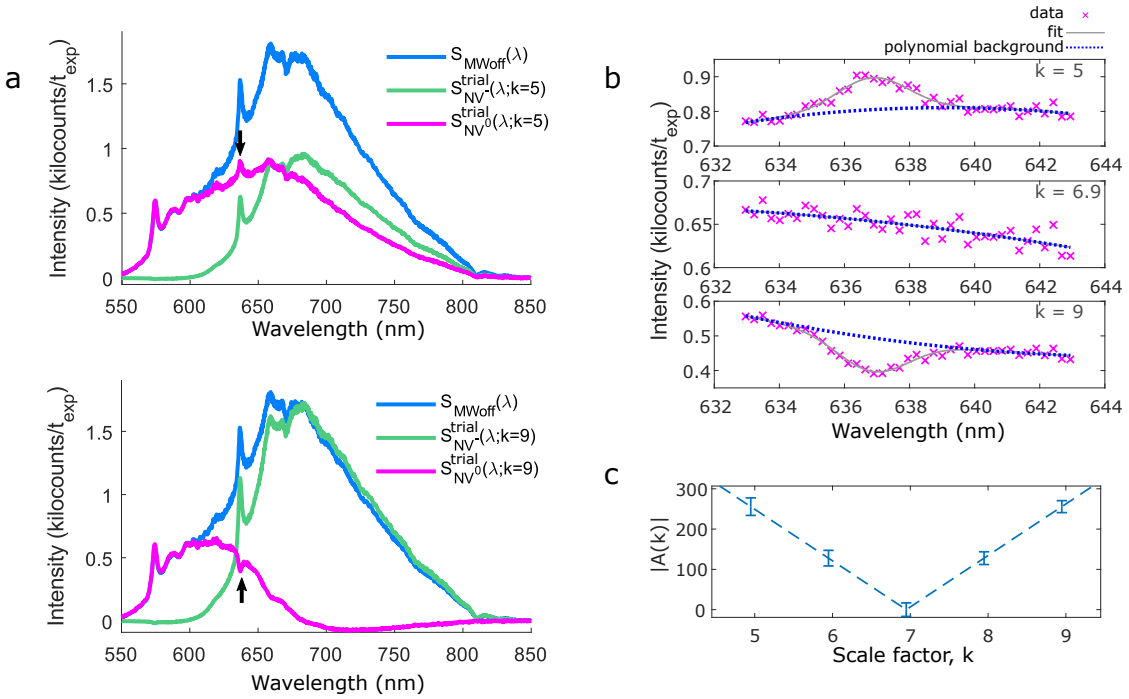


FIG. 3. The difference spectrum must be scaled by an unknown factor, k, to yield the NV^- contribution to the spectrum, $S^{\text{trial}}_{\text{NV}^-}(\lambda;k) = kS_{\text{diff}}(\lambda)$. The extracted NV^0 spectrum, found by subtracting the NV^- spectrum from the total microwaves-off spectrum, $S^{\text{trial}}_{\text{NV}^0}(\lambda;k) = S_{\text{MWoff}}(\lambda) - kS_{\text{diff}}(\lambda)$, should contain no NV^- ZPL signature at 637 nm when the scale factor k is chosen correctly. (a) Total spectrum (blue) and trial NV^- (green) and NV^0 (magenta) spectra for scale factors $k = 5 \ll k_0$ (top) and $k = 9 \gg k_0$ (bottom), where k_0 is the correct scale factor (for the NV ensemble analyzed here, $k_0 = 6.9$). For k smaller (larger) than the correct value k_0, a peak (dip) is seen in the extracted NV^0 spectrum at the NV^- ZPL wavelength, as indicated by the black arrows. (b) The trial NV^0 spectrum (magenta crosses) in the wavelength range around the NV^- ZPL is fitted with a Gaussian lineshape on a polynomial background (total fit function shown as solid line in gray and polynomial background shown as a dotted line in blue) for $k = 5 \ll k_0$ (top), $k = k_0 = 6.9$ (middle) and $k = 9 \gg k_0$ (bottom). Of the Gaussian's fit parameters, only the area, $A(k)$, is floated, since the width and center are fixed to match those of the NV^- ZPL. (c) Fitted area under the Gaussian peak/dip, $|A(k)|$ as a function of scale factor k. The area is minimized at the correct scale factor, $k = k_0 = 6.9$.

A. Isolating the NV^- spectral shape by microwave modulation

A series of photoluminescence spectra are taken under continuous 532-nm illumination, with alternating spectra taken with microwaves on and off (Fig. 1(b). To select the microwave-drive frequency at which we operate, we take an ODMR spectrum before acquiring the series of PL spectra (see Fig. 6 in the technical supplement) and set the microwave frequency to be resonant with one of the $m_s = 0$ to $m_s = \pm 1$ transitions.

In our example demonstration, we work at zero applied magnetic field (but do not cancel the Earth's field), where the splitting in energy between $m_s = +1$ and $m_s = -1$ spin states is small (here, a few MHz) and predominantly caused by local effects (most likely random lo-

cal electric fields, as discussed in [20]). Due to the absence of a sufficiently strong magnetic field, the ODMR resonances of all NV orientations are near-degenerate (see Fig. 6, inset), and all orientations are hence addressed by our microwave drive. Note however that, with an applied magnetic field oriented such that it splits the ODMR lines of different NV orientations, our method can also be used to selectively determine charge state of an ensemble of NVs oriented along one chosen axis.

When applied to the NV ensemble, the resonant microwave drive transfers population between the bright $m_s = 0$ state and the dimmer $m_s = \pm 1$ states, modulating the fluorescence emitted by NV^- whilst having no effect on NV^0 fluorescence (Fig. 1(a). By taking the difference between successive PL spectra measured with microwaves on and off, it is hence possible to isolate the spectral shape of the NV^- contribution to the detected fluorescence. We define the difference spectrum, $S_{\text{diff}}(\lambda)$, as:

$$S_{\text{diff}}(\lambda) = S_{\text{MWoff}}(\lambda) - S_{\text{MWon}}(\lambda) \qquad (4)$$

where $S_{\text{MWon}}(\lambda)$ and $S_{\text{MWoff}}(\lambda)$ are the spectra taken with microwaves on and off respectively, averaged over the series. Typically, between 2000 and 20,000 spectra are taken to average out the effect of shot-to-shot laser-intensity drift. This averaging, along with the use of a noise-eater circuit on the excitation path (Thorlabs NEL01), reduces the contribution of shot-to-shot intensity fluctuations to the difference spectrum to under 0.05%.

Once the difference spectrum is extracted, the NV^- and NV^0 spectra can be written as

$$S^{\text{trial}}_{\text{NV}^-}(\lambda; k) = k \times S_{\text{diff}}(\lambda) \qquad (5)$$

$$\begin{aligned} S^{\text{trial}}_{\text{NV}^0}(\lambda; k) &= S_{\text{MWoff}}(\lambda) - S^{\text{trial}}_{\text{NV}^-}(\lambda; k) \\ &= S_{\text{MWoff}}(\lambda) - k S_{\text{diff}}(\lambda) \end{aligned} \qquad (6)$$

where the "trial" subscript denotes that these are not the final spectral shapes, as they will later be modified by a correction for spin-dependent ionization (section II C), and k denotes a scale factor, to be determined in section II B. Note that k cannot simply be determined by measuring the NV^- ODMR contrast because, without knowledge of the ratio of charge state concentrations in the spot being illuminated, it is not possible to determine by how much we dim the NV^- fluorescence when the microwaves are turned on (we can only establish by how much we dim the total fluorescence). The measured difference spectrum of our example NV ensemble is shown in Fig. 2.

B. Finding the correct scale factor

We can now iterate the scale factor k and examine the resulting NV^0 spectra, $S^{\text{trial}}_{\text{NV}^0}(\lambda; k)$, we obtain by evaluating eq. 6 for each value of k. Since the NV^- zero phonon line (ZPL) at 637 nm is a defining feature of the NV^- emission spectrum that should not appear in the NV^0 spectrum, we can find the correct scale factor k by minimizing the area under any residual NV^- ZPL feature in $S^{\text{trial}}_{\text{NV}^0}(\lambda; k)$ (Fig. 3). We first find the width and center wavelength of the NV^- ZPL by fitting the NV^- ZPL on the microwaves-off spectrum with a Gaussian lineshape on a polynomial background. We then scan k and fit $S^{\text{trial}}_{\text{NV}^0}(\lambda; k)$ for a Gaussian feature of the same width and center wavelength as the NV^- ZPL; we select $k = k_0$, where k_0 minimizes the area, A, under this Gaussian, i.e., $A(k_0) = \min(A(k))$ (Fig. 3b,c). From eqs. 5 and 6, we can now evaluate trial NV^- and NV^0 spectra, $S^{\text{trial}}_{\text{NV}^-}(\lambda, k_0)$ and $S^{\text{trial}}_{\text{NV}^0}(\lambda, k_0)$.

C. Correcting for spin-dependent ionization

The $NV^- \rightarrow NV^0$ ionization rate may be different for populations in the $m_s = 0$ and $m_s = \pm 1$ states, so the relative NV^- and NV^0 concentrations can change when the microwave drive is applied. We observe this to be typically a small effect in our samples (once corrected for, it leads to $\lesssim 10\%$ change in the area of the difference spectrum). However, its magnitude does appear to vary from site to site in the

diamond, indicating that the effect is sensitive to the local lattice environment. For the NV ensemble studied here, illuminated with 2 mW 532-nm light on a diffraction-limited confocal spot, we observe an increase in the NV^0 population when the microwave drive is on. This manifests as an increased NV^0 fluorescence in the microwaves-on spectrum ($S_{\mathrm{MWon}}(\lambda)$), leading to a negative portion of the difference spectrum in the wavelength range around the NV^0 ZPL ($\sim$550 nm to 590 nm), where most of the fluorescence is contributed by NV^0. We postulate that the effect may stem from the fact that the microwave drive increases the population in the metastable singlet state, from whence NV^- may ionize with a different intensity-dependent rate than that with which it ionizes when in the excited ^3E state. We observe that the magnitude and sign of the effect is laser-power dependent; and we further study and discuss the power-dependence of this ionization effect in [21].

Because, for the dataset analyzed here, the NV^0 concentration is higher when the microwave drive is on, there is more NV^0 fluorescence contributing to the microwaves-on spectrum, $S_{\mathrm{MWon}}(\lambda)$, than to the microwaves-off spectrum, $S_{\mathrm{MWoff}}(\lambda)$. Hence, the difference spectrum, $S_{\mathrm{diff}}(\lambda) = S_{\mathrm{MWoff}}(\lambda) - S_{\mathrm{MWon}}(\lambda)$, contains a small, negative NV^0 fluorescence contribution. Note however, that the NV^0 spectrum we extracted in step 2, $S^{\mathrm{trial}}_{\mathrm{NV^0}}(\lambda, k_0)$, consists purely of NV^0 fluorescence by definition, since we selected the scale factor k_0 which eliminates any NV^- signature in the NV^0 spectrum. To see this, we can rewrite the difference spectrum as:

$$S_{\mathrm{diff}}(\lambda) = cS_{\mathrm{NV^-}}(\lambda) - \delta S_{\mathrm{NV^0}}(\lambda) \qquad (7)$$

where c and δ are scalar, positive constants and $S_{\mathrm{NV^0}}(\lambda), S_{\mathrm{NV^-}}(\lambda)$ are the NV^0 and NV^- components of the microwaves-off spectrum, as defined in eq. 3. Then, the trial NV^0 spectrum we extracted in step 2 can be written as:

$$\begin{aligned} S^{\mathrm{trial}}_{\mathrm{NV^0}}(\lambda; k_0) &= S_{\mathrm{MWoff}} - k_0 S_{\mathrm{diff}}(\lambda) \\ &= (1 + k_0\delta)S_{\mathrm{NV^0}}(\lambda) \\ &\quad +(1 - k_0 c)S_{\mathrm{NV^-}}(\lambda) \end{aligned} \qquad (8)$$

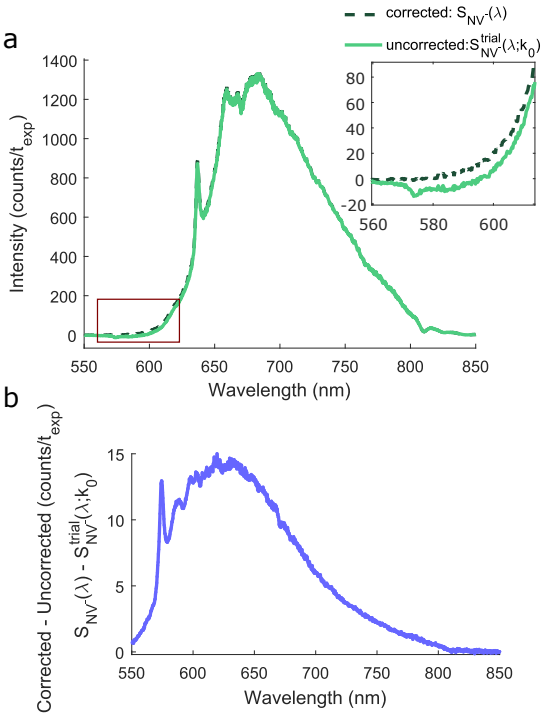


FIG. 4. a)Trial NV^- spectrum, $S^{\mathrm{trial}}_{\mathrm{NV^-}}$, before correction for spin-dependent ionization (light green solid line), and the corrected NV^- spectrum, $S_{\mathrm{NV^-}}$ (dark green dashed line). Inset shows the spectrum plotted in the wavelength range around the NV^0 ZPL (indicated in the main plot by a red box). (b) Difference between corrected and uncorrected NV^- spectra ($S_{\mathrm{NV^-}}(\lambda) - S^{\mathrm{trial}}_{\mathrm{NV^-}}(\lambda; k_0)$). Qualitatively, most of the contribution to this difference appears to come from NV^0 fluorescence – note the prominent peak at the NV^0 ZPL wavelength.

Note, however, that we chose $k = k_0$ such that there was no NV^- contribution $S^{\mathrm{trial}}_{\mathrm{NV^0}}$, i.e. $(1 - k_0 c) = 0$. Hence,

$$S^{\mathrm{trial}}_{\mathrm{NV^0}}(\lambda; k_0) = (1 + k_0\delta)S_{\mathrm{NV^0}}(\lambda) \qquad (9)$$

We can therefore correct $S^{\mathrm{trial}}_{\mathrm{NV^0}}(\lambda; k_0)$ simply by re-scaling it to match the microwaves-off spectrum in the wavelength region where only NV^0 fluoresces; i.e., we effectively divide $S^{\mathrm{trial}}_{\mathrm{NV^0}}(\lambda; k_0)$ by $(1 + k_0\delta)$ to obtain the correct NV^0 spectrum, $S_{\mathrm{NV^0}}(\lambda)$. Finally, we sub-

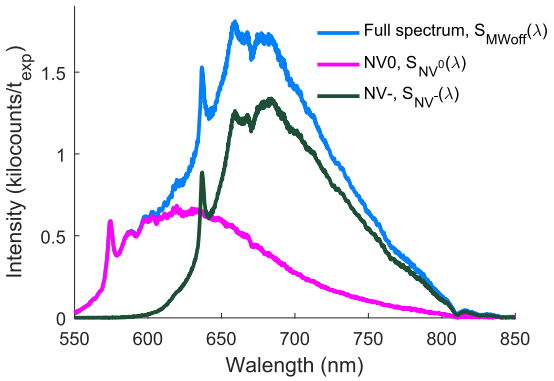


FIG. 5. Spectral decomposition (for our measurement and illumination conditions) of our measured NV ensemble spectrum (blue) into an NV^- contribution, $S_{NV^-}(\lambda)$, (dark green) and an NV^0 contribution, $S_{NV^0}(\lambda)$ (magenta). From the area under $S_{NV^0}(\lambda)$ and $S_{NV^-}(\lambda)$, we establish that 38(1)% of the fluorescence of this NV ensemble was contributed by NV^- defects and 62(1)% by NV^0 defects.

tract the corrected NV^0 spectrum from the total microwaves-off spectrum to yield a corrected NV^- spectrum, $S_{NV^-}(\lambda) = S_{MWoff}(\lambda) - S_{NV^0}(\lambda)$. Fig. 4 plots both the corrected and trial NV^- spectra, $S^-_{NV}(\lambda)$ and $S^{trial}_{NV^0}(\lambda; k_0)$ for our example NV ensemble data. Fig. 5 plots the NV ensemble's spectral decomposition into NV^- and NV^0 fluorescence contributions.

III. DISCUSSION

The method of charge-state-ratio determination presented here benefits from being tailored to the sample and experimental conditions under investigation. The extraction of the NV^- and NV^0 spectra in situ ensures that our measurement of charge-state ratio accounts for any changes in the shape the of the NV^- and NV^0 spectra due to sample-specific material properties (such as local strain) or experimental parameters (such as temperature and excitation wavelength). We note that the use of charge-state-determination methods that do not account for changes in the NV^- and NV^0 spectral shape – such as methods that decompose a sample spectrum by doing least-squares fitting with literature-reported NV^- and NV^0 spectra extracted from a different sample, or methods that compare the area under the NV^- and NV^0 ZPLs to extract charge-state ratio – are likely to yield inaccurate results. The former approach assumes no change in the NV^- and NV^0 fluorescence spectra across different samples and experimental setups; and the latter relies on a fixed (or, at least, known) proportion of the total fluorescence from each charge state being emitted in the ZPL. However, both spectral shape and proportion of fluorescence in the ZPL may vary from sample to sample and even from site to site in a given diamond. It is hence difficult to compare charge-state measurements by these methods across different samples. This in turn limits the usefulness of such methods in the identifying which material and experimental parameters can be tuned to produce the NV^--rich diamonds needed for high-sensitivity magnetometry.

The method presented here produces charge-ratio measurements that can be compared across different diamond samples and experimental conditions. In particular, it allows the investigation of charge-state ratio under any illumination sequence that optically pumps the NV^- state to $m_s = 0$ and produces a fluorescence contrast between the $m_s = 0$ and $m_s = \pm 1$ states of NV^-. This permits the investigation of charge-state ratio as a function of illumination duration, intensity and wavelength.

Further, our approach allows us to accurately describe the NV^- ^3E to $^3A_2$ (and NV^0 $^2A_2$ to ^2E) phonon sidebands, without contamination from the phonon sidebands of the other charge state. This can yield more accurate one-phonon spectra, from which we can obtain a better understanding of the NV vibrational modes and electronic wave functions [22].

The analysis presented here may also be adapted to work with other methods of selectively modulating NV^- fluorescence, such as magnetic-field-induced spin-polarization quenching [16].

Finally, the method we describe may be applied to determine concentration ratios and isolate spectra of other fluorescent solid-state defects (such as V1 and V2 silicon vacancies in silicon carbide [23]), facilitating the study of their optical and spin properties.

IV. ACKNOWLEDGMENTS

This work was partially supported by the NSF STC Center for Integrated Quantum Materials, NSF Grant No. DMR-1231319, Air Force Office of Scientific Research award FA9550-17-1-0371, Army Research Office grant W911NF-15-1-0548 and by NSF EAGER grant ECCS 1748106. J.M.S. was supported by a Fannie and John Hertz Foundation Graduate Fellowship and a National Science Foundation Graduate Research Fellowship under Grant No. 1122374.

V. TECHNICAL SUPPLEMENT

The experiments described here were performed on a home-built confocal microscope featuring a 10x objective lens of numerical aperture 0.28.

The excitation light was provided by a 532-nm diode-pumped solid-state laser (Coherent Verdi V10), which was focused onto a diffraction-limited spot on the diamond. The laser intensity was stabilized by a commercial noise-eater circuit (Thorlabs NEL01). For the data shown here, 2mW of laser power were focused onto the diamond.

NV fluorescence (separated from the excitation light by a dichroic filter) was passed through a grating spectrometer (Acton Research Corporation SpectraPro -500) and collected on a liquid-nitrogen-cooled CCD (Roper Scientific LN/CCD-1340/400-EB/1).

The microwave drive was provided by a signal generator (SRS 384) and applied to the diamond through a small loop antenna (~ 1 mm diameter). In our example demonstration of our charge-state determination method, 3.8W of microwave power at 2.873 GHz were fed to the antenna. A TTL-triggered microwave switch (Minicircuits ZASWA-2-50DR+) was used to turn on and off the microwave drive for the acquisition of microwaves-on and microwaves-off spectra in quick succession.

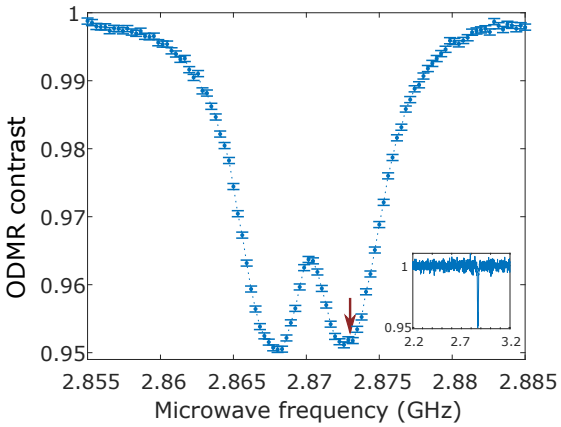


FIG. 6. ODMR spectrum for our example NV-diamond ensemble, acquired by scanning the frequency of the microwave drive and recording the fluorescence emitted by the NVs with an avalanche photodiode (under 2mW, 532-nm laser illumination, 3.8W of applied microwave power and no applied magnetic field). When the microwave drive frequency is resonant with one of the $m_s = 0$ to $m_s = \pm 1$ transitions, population is transferred from the bright $m_s = 0$ state to the dimmer $m_s = \pm 1$ states, causing a drop in NV fluorescence. The ODMR contrast is given by the ratio of the number of photons emitted by the NV ensemble when the microwave drive is on to that when the microwave drive is off. The red arrow indicates the microwave drive frequency, 2.873 GHz , applied in our example demonstration of the charge-state determination method. The inset shows an ODMR spectrum taken over a wider range of microwave frequencies.

A multi-channel TTL pulse generator (Spincore PulseBlaster), controlled by an expanded version of the qdSpectro Python package [24], was used to synchronously trigger CCD exposures and the microwave switch. The spectra obtained here were averaged over a series of 20,000 CCD frames, with subsequent acquisi-

tions taken with microwaves on and microwaves off. The CCD was exposed for an exposure time of $t_{\mathrm{exp}} = 100\,\mathrm{ms}$ to acquire each frame.

Data was collected with no applied magnetic field (except for the Earth's field, which was not canceled). To determine the resonance frequency at which the microwave drive should be applied, an ODMR spectrum (Fig. 6) was acquired before the series of PL spectra was taken. The microwave drive frequency was chosen to match an ODMR resonance.

The diamond used for the experiments presented here was provided by Element Six. It contains a $10\,\mu$m-thick NV layer ($10\,\mathrm{ppm}$ ^{14}N, $>99.95\%$ ^{12}C) grown by chemical vapor deposition (CVD) on an electronic-grade single-crystal substrate. This sample was irradiated with a dosage of 6×10^{18} electrons/cm^2 and annealed for 12 hours at $800\,^{\circ}\mathrm{C}$ and for 12 hours at $1000\,^{\circ}\mathrm{C}$.

[1] R. Schirhagl, K. Chang, M. Loretz, and C. L. Degen, Annual Review of Physical Chemistry **65**, 83 (2014).

[2] K. Jensen, P. Kehayias, and D. Budker, in *High Sensitivity Magnetometers, Smart Sensors, Measurement and Instrumentation*, edited by A. Grosz, M. J. Haji-Sheikh, and S. C. Mukhopadhyay (Springer International Publishing, Swtzerland, 2017) Chap. 18, pp. 553–576.

[3] F. Casola, T. van der Sar, and A. Yacoby, *Nature Reviews Materials*, **3**, 17088 (2018).

[4] D. Le Sage, K. Arai, D. Glenn, S. DeVience, L. Pham, L. Rahn-Lee, M. Lukin, A. Yacoby, A. Komeili, and R. Walsworth, Nature **496**, 486 (2013).

[5] D. Glenn, K. Lee, H. Park, R. Weissleder, A. Yacoby, M. D Lukin, H. Lee, R. Walsworth, and C. B Connolly, *Nature Methods*, **12** (2015).

[6] H. C. Davis, P. Ramesh, A. Bhatnagar, A. Lee-Gosselin, J. F. Barry, D. R. Glenn, R. L. Walsworth, and M. G. Shapiro, ArXiv e-prints (2016), arXiv:1610.01924 [physics.med-ph].

[7] J. F. Barry, M. J. Turner, J. M. Schloss, D. R. Glenn, Y. Song, M. D. Lukin, H. Park, and R. L. Walsworth, Proceedings of the National Academy of Sciences **113**, 14133 (2016).

[8] R. R. Fu, B. P. Weiss, E. A. Lima, P. Kehayias, J. F. Araujo, D. R. Glenn, J. Gelb, J. F. Einsle, A. M. Bauer, R. J. Harrison, G. A. Ali, and R. L. Walsworth, Earth and Planetary Science Letters **458**, 1 (2017).

[9] B. P. Weiss, R. R. Fu, J. Einsle, D. Glenn, P. Kehayias, E. Bell, J. Gelb, J. Araujo, E. Lima, C. Borlina, P. Boehnke, D. Johnstone, T. Mark Harrison, R. Harrison, and R. L. Walsworth, *Geology*, **46** (2018).

[10] T. Wolf, P. Neumann, K. Nakamura, H. Sumiya, T. Ohshima, J. Isoya, and J. Wrachtrup, Phys. Rev. X **5**, 041001 (2015).

[11] L. Robledo, H. Bernien, T. van der Sar, and R. Hanson, New Journal of Physics **13**, 025013 (2011).

[12] N. Aslam, G. Waldherr, P. Neumann, F. Jelezko, and J. Wrachtrup, New Journal of Physics **15**, 013064 (2013), arXiv:1209.0268 [quant-ph].

[13] X.-D. Chen, C.-L. Zou, F.-W. Sun, and G.-C. Guo, Applied Physics Letters **103**, 013112 (2013).

[14] P. Ji, R. Balili, J. Beaumariage, S. Mukherjee, D. Snoke, and M. V. G. Dutt, Phys. Rev. B **97**, 134112 (2018).

[15] N. Manson and J. Harrison, Diamond and Related Materials **14**, 1705 (2005).

[16] N. B. Manson, M. Hedges, M. S, J. Barson, R. Ahlefeldt, M. W. Doherty, M. J. Sellars, H. Abe, and T. Ohshima, ArXiv e-prints (2018), arXiv:1807.08889 [cond-mat.mtrl-sci].

[17] X.-D. Chen, C.-H. Dong, F.-W. Sun, C.-L. Zou, J.-M. Cui, Z.-F. Han, and G.-C. Guo, Applied Physics Letters **99**, 161903 (2011), https://doi.org/10.1063/1.3652910.

[18] T. L. McCormick, W. E. Jackson, and R. J. Nemanich, Journal of Materials Research **12**, 253263 (1997).

[19] J. Storteboom, P. Dolan, S. Castelletto, X. Li, and M. Gu, Opt. Express **23**, 11327 (2015).

[20] T. Mittiga, S. Hsieh, C. Zu, B. Kobrin, F. Machado, P. Bhattacharyya, N. Rui, A. Jarmola, S. Choi, D. Budker, and N. Y. Yao, ArXiv e-prints (2018), arXiv:1809.01668 [quant-ph].

[21] D. P. L. Aude Craik *et al*, in preparation (2018).

[22] P. Kehayias, M. W. Doherty, D. English, R. Fischer, A. Jarmola, K. Jensen, N. Leefer, P. Hemmer, N. B. Manson, and D. Budker, Phys. Rev. B **88**, 165202 (2013), arXiv:1301.6197 [physics.atom-ph].

[23] E. Janzén, A. Gali, P. Carlsson, A. Gällström, B. Magnusson, and N. Son, Physica B: Condensed Matter **404**, 4354 (2009).

[24] D. P. L. Aude Craik, "qdSpectro," `https://gitlab.com/dplaudecraik/qdSpectro` (2018), version 1.0.